2007

Moving Boundary Model for the Discharge of a LiCoO2 Electrode

Qi Zhang
University of South Carolina - Upstate, qhzhang@email.uscupstate.edu

Ralph E. White
University of South Carolina - Columbia, white@cec.sc.edu

Publication Info

Published in *Journal of the Electrochemical Society*, Volume 154, Issue 6, 2007, pages A587-A596.

Zhang, Q. & White, R.E. (2007). Moving Boundary Model for the Discharge of a LiCoO2 Electrode. *Journal of the Electrochemical Society*, *154*(6): A587-A596.
Publisher's Version: http://dx.doi.org/10.1149/1.2728733

Journal of The Electrochemical Society, **154** (6) A587-A596 (2007)
0013-4651/2007/154(6)/A587/10/$20.00 © The Electrochemical Society

Moving Boundary Model for the Discharge of a $LiCoO_2$ Electrode

Qi Zhang and Ralph E. White[*,z]

Department of Chemical Engineering, University of South Carolina, Columbia, South Carolina 29208, USA

A moving boundary model in a spherical $LiCoO_2$ particle is presented to account for the diffusion controlled phase transition in $LiCoO_2$ solid particles, and this model is incorporated into a porous electrode model for the $LiCoO_2$ electrode. The simulation results agree well with the experimental data of a $LiCoO_2$ electrode. A study of the flux distribution in the porous electrode shows that the phase transition phenomenon in the $LiCoO_2$ particles has a significant effect on the flux distribution by changing the solid phase diffusion resistance in the particles.
 [DOI: 10.1149/1.2728733]

Manuscript submitted December 13, 2006; revised manuscript received February 8, 2007. Available electronically April 30, 2007.

The intercalation reaction of $LiCoO_2$ has been extensively studied using X-ray diffraction (XRD), electrochemical analysis, and other physical measurements.[1-5] A characteristic feature of the intercalation reaction of $LiCoO_2$ is the so-called staging phenomenon,[5] which involves a series of phase transitions. Figure 1 presents a typical low rate discharge curve for a Li_xCoO_2 electrode, which includes a two phase region between $x = 0.75$ and $x = 0.975$. It is commonly agreed that the intercalation reaction of Li^+ ions into Li_xCoO_2 with x between 0.25 and 0.75 is a single phase reaction plus a subtle phase transition due to the formation of a monoclinic phase at $x \approx 0.5$ as shown in Fig. 1. Continuing the Li^+ intercalation reaction causes a two phase region to form at $x = 0.75$ and persist until $x = 0.975$ after which the electrode returns to a single phase. The existence of these two phases is indicated by the potential plateau shown in Fig. 1.

Moving boundary models have been used previously to study systems[6-10] characterized by phase coexistence or phase transition. Therefore, they could also be used to study the phase transition process in a $LiCoO_2$ particle, in particular as shown in the papers of Pyun and co-workers.[7,8] Figure 2 presents the sequences of lithium intercalation into a single $LiCoO_2$ particle during discharge described from the standpoint of a moving boundary model. The insertion reaction of a $LiCoO_2$ particle usually starts in the single phase reaction stage where the particle is occupied with Li poor α phase only. Lithium ions are reduced at the particle surface and then diffuse into Li poor α phase. Further insertion results in phase separation with the formation of a Li rich β phase shell surrounding a Li poor α phase core. These two phases with different lithium concentrations are separated by a moving phase boundary denoted as $r = r(t)$ in the figure. The insertion process at this stage involves lithium ion intercalation at the particle surface, movement of intercalated lithium ions first across the β phase shell, then across the phase boundary and finally into the α phase core. The phase boundary moves toward the center of the particle as the insertion process proceeds, causing the internal core to shrink and the external shell to expand. When the α phase core is completely consumed, the whole particle is fully occupied with β phase, where lithium ions are inserted in the same way as when the particle was occupied with α phase only.

Pyun and co-workers[7,8] used a phase boundary movement model to analyze the potentiostatic current transient response of lithium intercalation into a $LiCoO_2$ electrode. However, their model is based only on the behavior of a single $LiCoO_2$ particle and does not consider the porous nature of the electrode. In addition, their model does not quantitatively establish the current and potential relationship of a $LiCoO_2$ electrode. Consequently, their model cannot be used to predict discharge curves for a $LiCoO_2$ electrode at a given current. Srinivasan and Newman[10] used a shrinking core model to simulate discharge curves for a $LiFePO_4$ electrode. Their model used the assumption that a Li rich β phase shell forms immediately outside the undisturbed core when the discharge of a $LiFePO_4$ particle begins. The conceptual phase boundary movement for the shrinking core model is shown in Fig. 3. Note that the scenario described in Fig. 3 is quite different from that in Fig. 2. There is no single phase intercalation reaction stage before a core/shell structure forms in the shrinking core model. The concentration in the core is maintained at its initial concentration at all times; and consequently there is no concentration gradient in the undisturbed core. This simplified model cannot be used for the $LiCoO_2$ particles because of the existence of the α phase at the early stage of intercalation before the β phase is formed.

The moving boundary model and shrinking core model are "sharp interface" models[11] which explicitly track the position of a sharp phase boundary during phase transition. The concentration changes abruptly (a jump) at the phase boundary, as indicated in Fig. 2b and 3a. In contrast, the phase field model by Han et al.,[12] a diffuse interface approach,[11] describes the time evolution of a conserved concentration "field" using a Cahn-Hilliard formulation without explicitly tracking the interface position. The diffuse interface between the phases in the phase field model has a finite thickness and is described by smooth but highly localized changes of the field

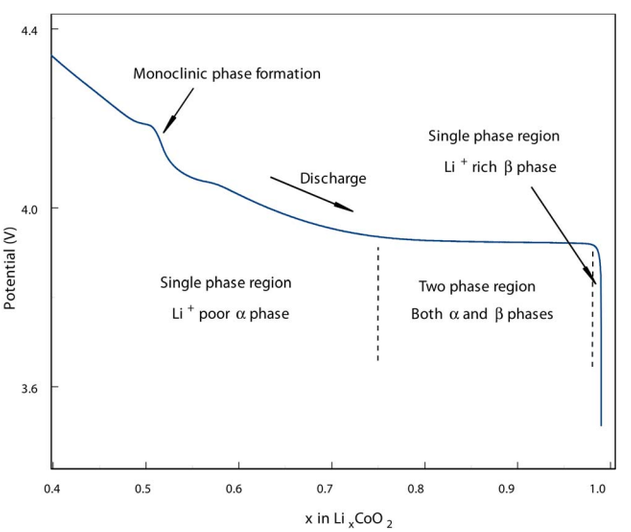

Figure 1. (Color online) A typical discharge profile of a $LiCoO_2$ electrode at very low discharge rate. The $LiCoO_2$ material undergoes a monoclinic phase formation, followed by formation of two phases at $x \approx 0.75$ and finally a transformation back to one phase at $x \approx 0.975$.

* Electrochemical Society Fellow.
z E-mail: white@engr.sc.edu

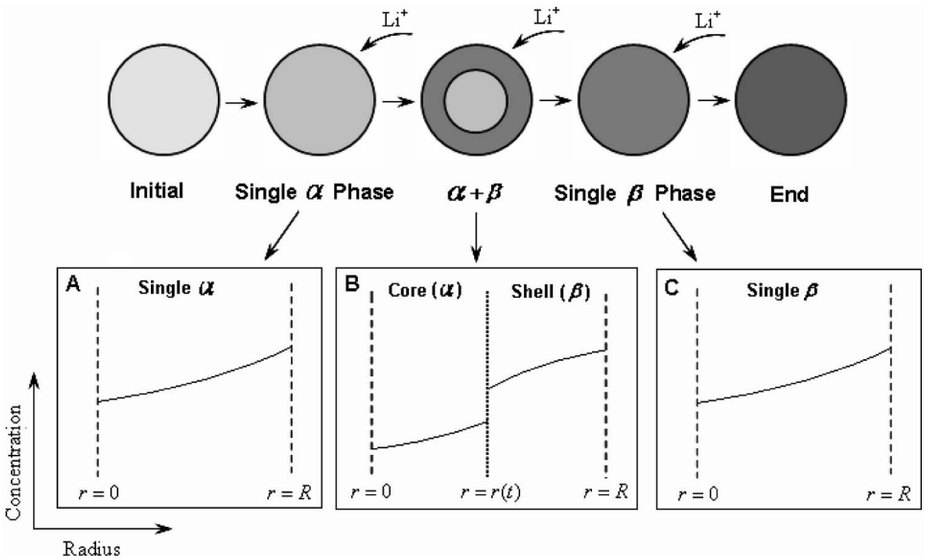

Figure 2. The intercalation process of Li^+ into a $LiCoO_2$ particle during discharge. The intercalation process goes through diffusion in single α phase stage (A), then phase transition stage (B), and finally diffusion in a single β phase stage (C).

variable, the concentration. The phase field model avoids the mathematically difficult problem of applying boundary conditions at a sharp interface whose location is part of the unknown solution. The authors[12] performed phase field simulations of galvanostatic intermittent titration technique (GITT) and potentiostatic intermittent titration technique (PITT) experiments for a $LiFePO_4$ electrode and concluded that phase field models could be used to study intercalation in electrodes with experimentally measured or calculated Fickian diffusion coefficients.

The model presented in this work incorporates the phase transition sequence in a $LiCoO_2$ particle through a moving boundary model into a full scale porous electrode model for the first time. The model is subsequently used to predict the experimental discharge curves at several rates for a $LiCoO_2$ electrode.

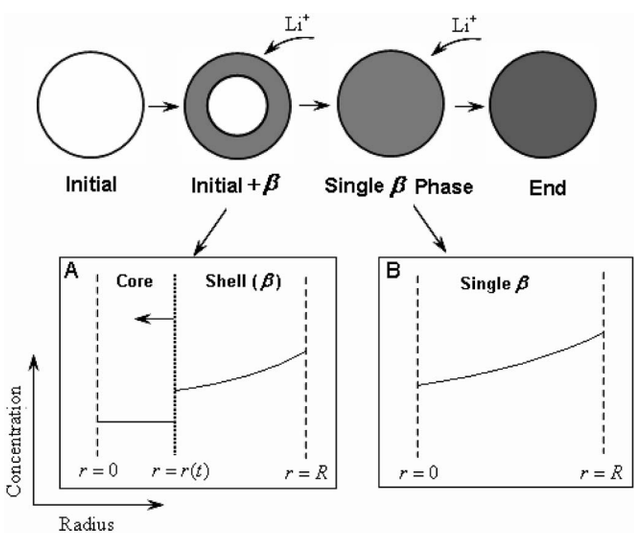

Figure 3. Schematic showing the phase boundary movement described with the shrinking core model. The model assumes that a core/shell structure forms immediately upon intercalation. The concentration in the core is maintained at its initial value and there is no concentration gradient inside the internal core at any time.

Experimental

The galvanostatic discharge profiles of a $LiCoO_2$ electrode were measured using a Swagelok-type half cell (see Fig. 4). The half cell consisted of a $LiCoO_2$ working electrode, a separator, and a lithium foil counter electrode. A cone-shaped piece of lithium metal with a sharp end was placed just above the $LiCoO_2$ electrode to serve as the reference electrode. The half cell setup provided a means of measuring the potential of the $LiCoO_2$ electrode vs the Li/Li^+ reference electrode shown in Fig. 4. The working $LiCoO_2$ electrode was a round disk with a diameter of 0.5 in. punched out of a single-sided $LiCoO_2$ sheet electrode provided by Mine Safety Appliances (Sparks, MD). A Celgard-2300 polypropylene membrane (Charlotte, NC) with a thickness of 25 μm was used as the separator. The electrolyte (Ferro, Independence, OH) was 1.0 M $LiPF_6$ in a solvent mixture of ethylene carbonate/polycarbonate/ethylmethyl carbonate/diethyl carbonate (EC/PC/EMC/DEC). The half cell was assembled in an argon-filled glovebox, then removed and placed in a Tenney environmental chamber controlled at 15°C. An 8-channel Arbin battery test unit was used to conduct the experiment.

The half cell was first cycled several times at the C/13 rate (C = 4 mA) between 3.0 and 4.35 V vs Li/Li^+ to stabilize the electrode performance. The capacity of the $LiCoO_2$ disk electrode was measured to be around 4 mAh when cycled in the given voltage window (3.0–4.35 V vs Li/Li^+). Rate capability tests were then conducted to obtain the galvanostatic discharge profiles of the $LiCoO_2$ electrode.

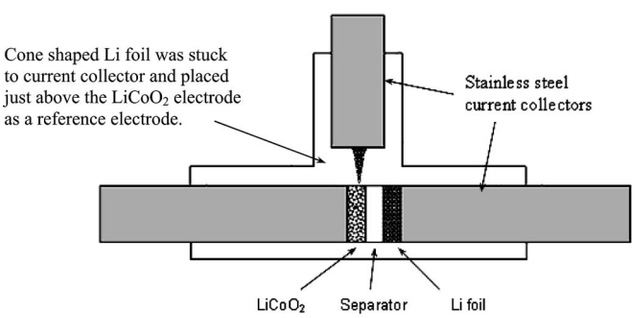

Figure 4. Schematic of a $LiCoO_2$ half cell setup used in the experiment. A reference electrode was used to measure the potential of the $LiCoO_2$ electrode.

The currents used in the test were 6×10^{-5}, 3×10^{-4}, 6×10^{-4}, 1.5×10^{-3}, and 3×10^{-3} A, which correspond roughly to C/66, C/13, C/7, C/2.7, and C/1.3 rates, respectively. For the test at the C/66 rate, a single stage constant current protocol was used to charge and discharge the cell to the desired voltage. For other rates, a two-stage constant current protocol was used. The cell was first charged or discharged to the desired voltage using the target rate. Then, a small current (C/66 rate) was applied to continue charge or discharge until the desired voltage was reached once again. The use of the two stage protocol ensured that the cell reached the same SOC at the beginning of charge or discharge at different current rates.

Model Development

Porous electrode models[13-15] have been used heavily in the literature to study lithium-ion cells. The advantage of the porous electrode model is that it considers the effects of both the solid phase and the liquid phase, which makes the model comprehensive. A detailed explanation of the porous electrode model can be found elsewhere.[14,15] The model equations are summarized below for the convenience of the reader. The model equations consist of mass transport equation (Eq. 1) and modified Ohm's law equation (Eq. 2) for the solution phase, Ohm's law equation (Eq. 3) for the solid phase, and the Butler Volmer equation (Eq. 4) for intercalation reaction which connects the concentrations and potentials in the solid and solution phases

$$\frac{\partial \varepsilon_e c_e}{\partial t} - \nabla \cdot (D_e^{\text{eff}} \nabla c_e) - \frac{1 - t_+^0}{F} a_s j_n = 0 \quad [1]$$

$$\nabla \cdot \left(\kappa_e^{\text{eff}} \nabla \phi_e - \frac{2RT\kappa_e^{\text{eff}}}{F}(1 - t_+^0)\left(1 + \frac{d \ln f_\pm}{d \ln c_e}\right) \nabla \ln c_e \right) + a_s j_n = 0 \quad [2]$$

$$\nabla \cdot (\sigma_s \nabla \phi_s) - a_s j_n = 0 \quad [3]$$

$$j_n = i_0 \left(\exp\left(\frac{\alpha_a F}{RT}(\phi_s - \phi_e - U_{eq}) \right) - \exp\left(-\frac{\alpha_c F}{RT}(\phi_s - \phi_e - U_{eq}) \right) \right) \quad [4a]$$

$$i_0 = k c_e^{\alpha_a} (c_{\max} - c|_{r=R_s})^{\alpha_a} c|_{r=R_s}^{\alpha_c} \quad [4b]$$

The Butler-Volmer equation requires knowledge of the lithium concentration at the surface of local particles $c|_{r=R_s}$, which is typically obtained by solving Fick's diffusion equation for lithium transport in the solid phase. Fick's diffusion law can be used to describe the lithium ion transport process if there is only one single phase in a $LiCoO_2$ particle. But when the phase transition occurs, the intercalated lithium ions need to first move across the β phase shell, then across the phase boundary, and finally into the α phase core. Hence, the lithium transport in the particle must be described with a mechanism significantly different from that in the presence of only a single phase.

In the following, we present a model which integrates the moving boundary model into the porous electrode model to account for the phase transition in $LiCoO_2$ particles and the porous nature of a $LiCoO_2$ electrode. The schematic of the cell modeled in this study is shown in Fig. 5. The cell consists of a $LiCoO_2$ positive electrode, a porous separator, and a Li foil negative electrode. Coordinates x and r are labeled for the direction across the cell and the particles, respectively.

The discharge of a $LiCoO_2$ electrode is assumed to start in single α phase reaction stage. Figure 6 presents a sketch of the lithium ion concentration profiles inside a $LiCoO_2$ particle during discharge. Li ions diffuse into the single α phase and the transport process is governed by Fick's diffusion law in the entire particle domain $\Omega_\alpha = [0, R_s]$

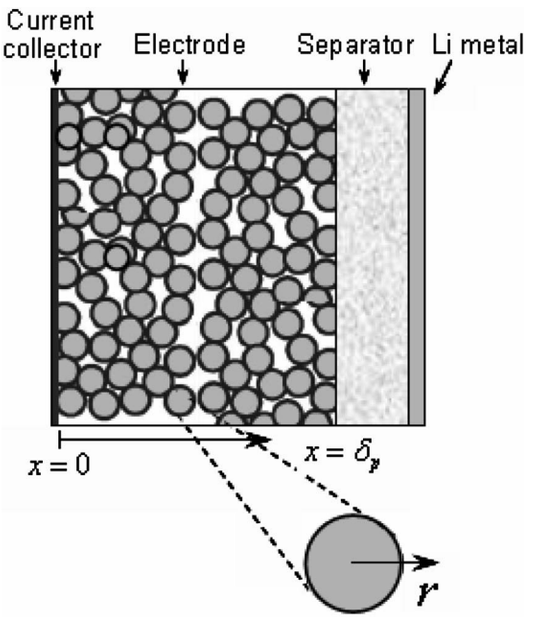

Figure 5. Schematic of a $LiCoO_2$ half cell sandwich, consisting of $LiCoO_2$ electrode, separator and lithium foil anode (from left to right). Coordinates x and r are labeled for the direction of the cell and the particles, respectively.

$$\frac{\partial c_\alpha}{\partial t} = \frac{1}{r^2}\left(D_\alpha r^2 \frac{\partial c_\alpha}{\partial r} \right) \quad [5a]$$

$$-D_\alpha \left.\frac{\partial c_\alpha}{\partial r}\right|_{r=0} = 0 \quad [5b]$$

$$-D_\alpha \left.\frac{\partial c_\alpha}{\partial r}\right|_{r=R_s} = \frac{j_n}{F} \quad [5c]$$

The boundaries are fixed at this stage of lithium transport and there is no phase boundary in the particles. The initial condition for Eq. 5 is the initial lithium concentration c_0 in the particles which can be readily calculated from the state of charge (SOC) of the $LiCoO_2$ electrode

$$c_\alpha|_{t=0} = c_0 \quad [5d]$$

When the concentration at the particle surface $c|_{r=R_s}$ reaches the maximum solubility limit of Li poor α phase $c_{eq,\alpha}$, a layer of Li rich β phase shell starts to form surrounding the Li poor α phase core upon further lithium ion intercalation. These two phases (α and β) are separated by a phase boundary which moves toward the center of a particle as the intercalation process proceeds. The particle thus enters into a two phase coexistence.

When the diffusion controlled phase transition occurs, the entire particle domain is divided into the internal α phase core $\Omega_\alpha = [0, r(t)]$ and the external β phase shell $\Omega_\beta = [r(t), R_s]$ where the position of the phase boundary $r(t)$ is a function of the discharge time. The lithium ion transport in the α phase core $\Omega_\alpha = [0, r(t)]$ is governed by diffusion and can be described by Fick's law

$$\frac{\partial c_\alpha}{\partial t} = \frac{1}{r^2}\left(D_\alpha r^2 \frac{\partial c_\alpha}{\partial r} \right) \quad [6a]$$

$$-D_\alpha \left.\frac{\partial c_\alpha}{\partial r}\right|_{r=0} = 0 \quad [6b]$$

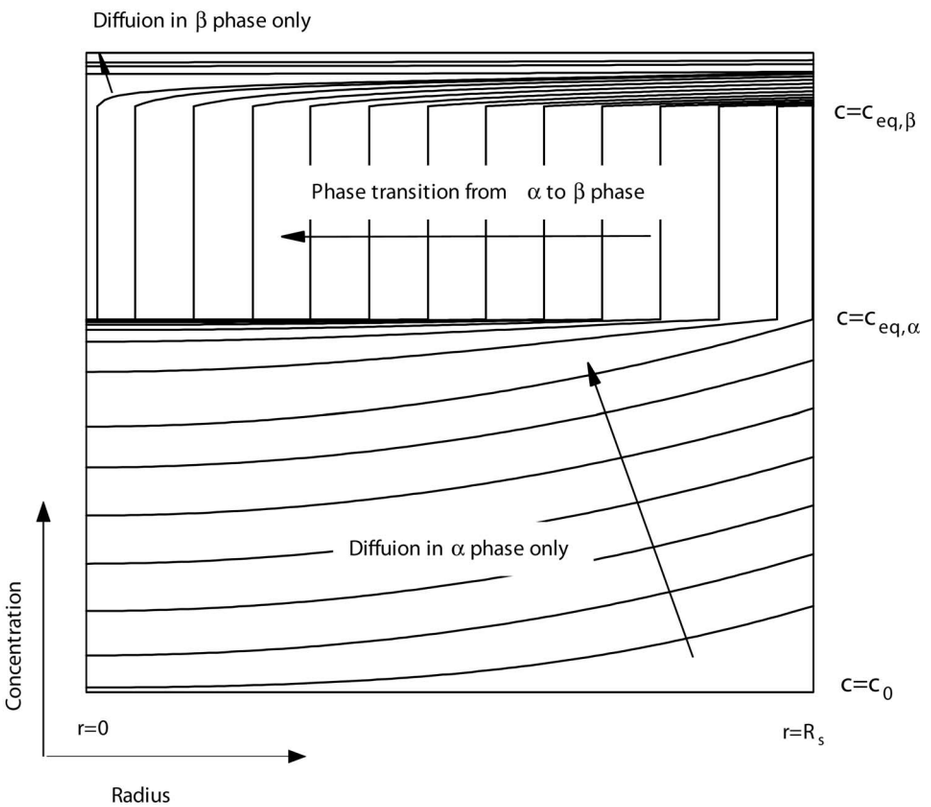

Figure 6. Schematic showing the lithium ion concentration profiles in a $LiCoO_2$ particle during discharge. Phase transition occurs when the surface concentration reaches $c_{eq,\alpha}$. The vertical lines indicate the position of the phase boundary. Phase transition ends when the phase boundary reaches the center of the particle.

$$c_\alpha|_{r=r(t)} = c_{eq,\alpha} \quad [6c]$$

where $c_{eq,\alpha}$ is set according to the experimental data and $c_{eq,\alpha} = 0.75 \times c_{max}$. The initial condition for Eq. 6 is the lithium concentration profile inside the particle taken when the surface concentration $c|_{r=R_s}$ reaches $c_{eq,\alpha}$. Meanwhile, the lithium transport in the β phase shell $\Omega_\beta = [r(t),R_s]$ can be described through

$$\frac{\partial c_\beta}{\partial t} = \frac{1}{r^2}\left(D_\beta r^2 \frac{\partial c_\beta}{\partial r}\right) \quad [7a]$$

$$c_\beta|_{r=r(t)} = c_{eq,\beta} \quad [7b]$$

$$-D_\beta \left.\frac{\partial c_\beta}{\partial r}\right|_{r=R_s} = \frac{j_n}{F} \quad [7c]$$

The initial condition for Eq. 7 is

$$c_\beta = c_{eq,\beta} \quad [7d]$$

where $c_{eq,\beta}$ is the minimum solubility of the Li rich β phase which is assumed to be in equilibrium with the maximum solubility of the Li poor α phase $c_{eq,\alpha}$ at the phase boundary $r(t)$. Here $c_{eq,\beta} = 0.975 \times c_{max}$. Note that not only the boundary conditions of Eq. 6 and 7 are different from those of Eq. 5, but also the boundaries are no longer fixed because the position of the phase boundary $r(t)$ changes with discharge time.

To solve Eq. 6 and 7, the time dependent position of the phase boundary has to be determined through a mass balance at the interface

$$D_\alpha \left.\frac{\partial c_\alpha}{\partial r}\right|_{r=r(t)^-} - D_\beta \left.\frac{\partial c_\beta}{\partial r}\right|_{r=r(t)^+} = [c_{eq,\beta} - c_{eq,\alpha}]\frac{dr(t)}{dt} \quad [8a]$$

This equation states that the difference of the lithium fluxes at the phase boundary drives the movement of the boundary. The phase boundary first appears at the particle surface, thus the initial condition for Eq. 8 is

$$r(t_0) = R_s \quad [8b]$$

which is practically a value close to R_s, i.e., $0.999 \times R_s$, is used for $r(t_0)$ in the simulation so that the diffusion equation for β phase shell (Eq. 7) can be solved.

When the phase boundary reaches the center of the particle $r(t) = 0$, the lithium ion transport is again governed by diffusion in the particle domain $\Omega_\beta = [0,R_s]$ which is instead filled with β phase only

$$\frac{\partial c_\beta}{\partial t} = \frac{1}{r^2}\left(D_\beta r^2 \frac{\partial c_\beta}{\partial r}\right) \quad [9a]$$

$$-D_\beta \left.\frac{\partial c_\beta}{\partial r}\right|_{r=0} = 0 \quad [9b]$$

$$-D_\beta \left.\frac{\partial c_\beta}{\partial r}\right|_{r=R_s} = \frac{j_n}{F} \quad [9c]$$

The initial condition for Eq. 9 is the lithium concentration profile in the β phase shell taken when the phase transition ends ($r(t) = 0$). Practically the phase transition is considered to be completed when $r(t)$ reaches $0.001 \times R_s$ in the simulation.

Equations 5-9 constitute a set of equations needed to account for the phase transition sequence in a $LiCoO_2$ particle during discharge. They are coupled to the porous electrode equations (Eq. 1-4) using a pseudo-two-dimensional approach.

Solution Procedure

Equations 6-8, which describe the diffusion controlled phase transition in a $LiCoO_2$ particle, constitute a moving boundary problem, also known as a Stefan problem.[16] Several methods[16-19] have been developed to solve moving boundary problems numerically. The Landau transformation method[16,17] is used in this work for its simplicity and ease of implementation.

The Landau transformation introduces two new positional variables (u and v), one for each phase. For the α phase core in the physical domain of $\Omega_\alpha = [0, r(t)]$, the spatial variable $u = r/r(t)$ is introduced to fix the boundaries of the α phase to the computational domain $0 \leqslant u \leqslant 1$. The governing equation in the α phase core (Eq. 6) can be rewritten in terms of u as follows

$$[ur(t)]^2\left(\frac{\partial c_\alpha}{\partial t} - \frac{u}{r(t)}\frac{dr(t)}{dt}\frac{\partial c_\alpha}{\partial u}\right) = \frac{\partial}{\partial u}\left(D_\alpha \frac{(ur(t))^2}{r(t)^2}\frac{\partial c_\alpha}{\partial u}\right) \quad [10a]$$

$$-D_\alpha \left.\frac{\partial c_\alpha}{\partial u}\right|_{u=0} = 0 \quad [10b]$$

$$c_\alpha|_{u=1} = c_{eq,\alpha} \quad [10c]$$

For the β phase shell in the physical domain of $\Omega_\beta = [r(t), R_s]$, the special variable $v = r - r(t)/R_s - r(t)$ is introduced to confine the boundaries of the β phase to the computational domain $0 \leqslant v \leqslant 1$. The governing equation in the β phase shell (Eq. 7) can be rewritten in terms of v as follows

$$[v(R_s - r(t)) + r(t)]^2\left(\frac{\partial c_\beta}{\partial t} - \frac{1-v}{R_s - r(t)}\frac{dr(t)}{dt}\frac{\partial c_\beta}{\partial v}\right) = \frac{\partial}{\partial v}\left(D_\beta \frac{[v(R_s - r(t)) + r(t)]^2}{[R_s - r(t)]^2}\frac{\partial c_\beta}{\partial v}\right) \quad [11a]$$

$$c_\beta|_{v=0} = c_{eq,\beta} \quad [11b]$$

$$-D_\beta \left.\frac{\partial c_\beta}{\partial v}\right|_{v=1} = \frac{j_n}{F}(R_s - r(t)) \quad [11c]$$

The transformed version of the phase boundary equation (Eq. 8) is

$$\frac{D_\alpha}{r(t)}\left.\frac{\partial c_\alpha}{\partial u}\right|_{u=1} - \frac{D_\beta}{R_s - r(t)}\left.\frac{\partial c_\beta}{\partial v}\right|_{v=0} = [c_{eq,\beta} - c_{eq,\alpha}]\frac{dr(t)}{dt} \quad [12]$$

Although the new coordinate system has rendered the governing equations (Eq. 10-12) into a more complex form than the original one, it has simplified the problem in that all of the computational domains are now fixed instead of changing with time. Consequently, numerical methods developed to solve systems of partial differential equations with fixed boundaries can be easily applied to this moving boundary problem. Because Eq. 5 and 9 have fixed physical boundaries when describing lithium transport in a single α or β phase, they do not need any transformation.

The lithium transport in a $LiCoO_2$ particle has been shown to have three distinct stages, namely, diffusion in single α phase, diffusion controlled phase transition from α phase to β phase, and diffusion in single β phase. Equations 5-9 describe such a lithium transport sequence for a single $LiCoO_2$ particle. Nevertheless, when these equations are coupled to the porous electrode model, the situation becomes even more complicated.

The porous electrode model is usually solved with spatial discretization along the x coordinate shown in Fig. 5 with finite difference or finite element technique. To obtain the lithium concentration at the local particle surface $c|_{r=R_s}$, the lithium transport equations (Eq. 5-9) for a $LiCoO_2$ particle have to be solved at each discretization point along the spatial x direction. The phase transition sequence in the entire $LiCoO_2$ electrode during discharge is shown in Fig. 7. Initially lithium transport in the particles is governed by diffusion in single α phase over the entire electrode (Fig. 7a). As discharge goes on, the particles close to the separator side ($x = \delta_p$) of the electrode will reach the phase transition threshold first because the intercalation current is higher there. Figure 7b shows that after the discharge process starts, some of the $LiCoO_2$ particles enter the diffusion controlled phase transition stage, while others are still in single α phase stage. Different sets of equations, as described above, are used to describe lithium ion intercalation and transport in the particles, according to their appropriate stages. Continued lithium ion insertion leads to diffusion controlled phase transition over the entire electrode followed by the gradual transition into diffusion in single β phase in the entire electrode as shown in Fig. 7c-e.

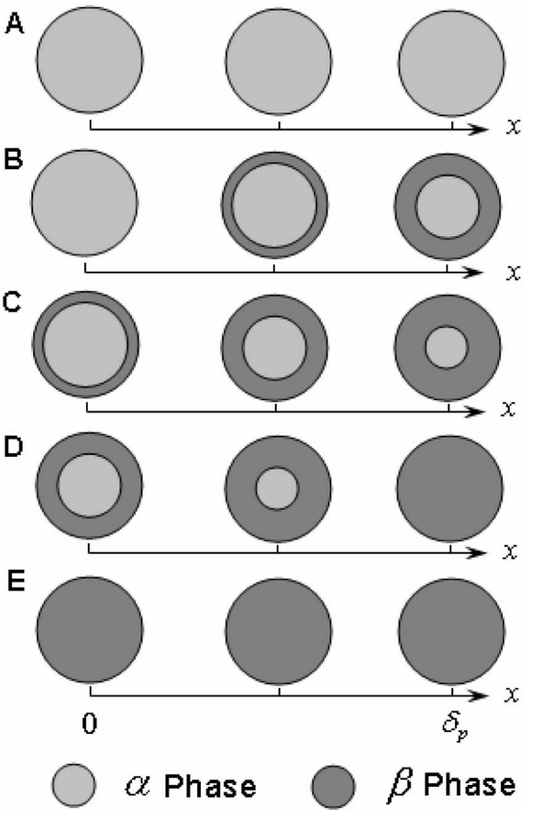

Figure 7. Schematic showing the phase transition sequences in a $LiCoO_2$ electrode during discharge. Stage A: diffusion in single α phase in all particles. Stage B: phase transition in some particles. Stage C: phase transition in all particles. Stage D: diffusion in single β phase in some particles. Stage E: diffusion in single β phase in all particles.

A summary of the model equations is listed in Table I. The equation sets were cast in finite difference form in both the x and r coordinates, which yields a pseudo-2D problem[14,15] consisting of differential and algebraic equations (DAEs).[20] The moving boundary equations are tightly coupled to the porous electrode equations, which requires solving all of the equations simultaneously. For example, when the entire $LiCoO_2$ electrode is in phase transition stage, the unknown variables to be determined in the $LiCoO_2$ electrode are $[c_{\alpha,1}, \cdots, c_{\alpha,m}, r(t), c_{\beta,1}, \cdots, c_{\beta,m}, j_n, c_e, \phi_s, \phi_e]_n$ where m nodes are used to discretize the fixed computational domain (Eq. 10 and 11) for the α and β phases, and n nodes are used in the x direction. The Fortran DAE solver DDASRT[20] was used to solve the resulting DAEs. The DDASRT solver uses a combination of backward differentiation formula and a choice of direct linear system solution methods to solve the system of DAEs. Time stepping is handled automatically by the solver. The root finding capability of the DDASRT solver is especially useful in this study because it was used to cap-

ture the critical events that happen in a local $LiCoO_2$ particle, namely, when the diffusion controlled phase transition starts ($c|_{r=R_s} = c_{eq,\alpha}$) or ends ($r(t) = 0$) in the particle.

Results and Discussion

The experimental galvanostatic discharge profiles of a $LiCoO_2$ electrode are presented in Fig. 8, where the electrode potential is plotted against x in Li_xCoO_2 where $x = 1$ represents a fully discharged electrode. The value of x in Li_xCoO_2 was calculated based on

$$x = x_0 + Q/(0.274 \times W) \quad [13]$$

where x_0 is the initial SOC of the $LiCoO_2$ electrode and was set equal to 0.393 in this study. This value of $x_0 = 0.393$ was determined based on the total charge capacity (4 mAh) and the active material loading (W) of the $LiCoO_2$ disk electrode. The discharge capacity Q in Ah was obtained directly from experimental data as the discharge current in Amps times the discharge time in hours. The factor of 0.274 in Eq. 13 is the theoretical capacity in Ah obtained by converting 1 g of $LiCoO_2$ completely to CoO_2, and W is the active material loading of the $LiCoO_2$ disk electrode which was determined to be around 0.0245 g based on the disk electrode size (0.5 in. disk) and the electrode loading data provided by the manufacturer (18.9 mg/cm^2). An important characteristic of the $LiCoO_2$ discharge profiles shown in Fig. 8 is that the voltage plateau that is well shaped at low rates gradually disappears at high rates. Similar phenomenon is also observed on a $LiFePO_4$ electrode.[10,21] Also shown in Fig. 8 are the predicted discharge curves obtained using the moving boundary model. The model parameters used in the simulation are listed in Table II. Simulation results show good agreement with the experimental data.

Most studies[25-30] reported that the diffusivity for Li_xCoO_2 in the composition range of $0.5 < x < 0.75$ is of the order of 10^{-11} to 10^{-9} cm^2/s. However, the diffusivity for the β phase is expected to be much smaller than that for the α phase.[10,11,25] As shown in Table II, the values of the diffusivity for the α and β phases used in the simulation agree to the studies from other groups. The kinetic constant (k_i) depends on which phase exists at the surface of the particles. The assumption seems reasonable because the two phases could have different properties. The values of the kinetic constants were determined by fitting to the experimental discharge curves. The quasi-equilibrium stoichiometries of the α and β phases ($c_{eq,\alpha}$ and $c_{eq,\beta}$) were fixed at 0.75 and 0.975, respectively, at the phase boundary. It is probable that the outer and inner phases during the diffusion controlled phase transition are not separated by a sharp phase boundary, but rather by a diffuse region between two pseudo phases in which the properties have not yet reached those of the bulk of either pseudo phase. However, we have not attempted to model this case. Instead, we have assumed that a sharp boundary exists between the phases. The transport properties of $LiPF_6$ in EC/PC/EMC/DEC system are taken from a study[31] where they are measured as a function of temperature and $LiPF_6$ concentration in comparable solvents, PC/EC/DMC mixture. Expressions for these transport properties for the electrolyte are listed in the Appendix.

The flux distribution across a $LiCoO_2$ electrode exhibits different patterns during discharge because of the phase transition phenomenon. The flux distribution which evolves over time is shown in Fig. 9 and 10 for C/1.3 and C/7 rates, respectively. When all the particles are occupied by the single α phase (Fig. 7a), the particle surface flux is larger at the separator side of the electrode, which means that more Li^+ ions are inserted into the particles close to the separator. Because of the uneven distribution of the intercalation reaction inside the electrode, the phase transition occurs earlier in the particles close to the separator than those close to the current collector (Fig. 7b). The ridges and valleys shown in stage A in Fig. 9 are caused by the small bump and dent in the low rate discharge curve (see Fig. 1) at $x = 0.5 \sim 0.6$. The ridge in stage B in Fig. 9 and 10 shows the gradual occurrence of the phase transition across the $LiCoO_2$ electrode. The location of the peak on the ridge indicates at what time and position in the electrode that the phase transition happens. The pattern of flux distribution is gradually inverted as the phase transition occurs in the electrode. The reaction "hot" region gradually shifts from the separator side of the electrode to the current collector side. The reason for the shift lies in the change of solid phase diffusion resistance in the particles in the electrode by the phase transition phenomenon. The diffusivity of Li ions in the β phase is much smaller than that in the α phase. Thus, when the particles close to the separator side become covered by a β phase shell, the local solid phase diffusion resistance increases dramatically, forcing the flux to move deeper into the electrode where the solid phase diffusion resistance is less. When all particles are in phase transition and covered by a β phase shell (stage C in Fig. 9 and 10), the β phase shells are thicker on the particles closer to the separator side, leading to larger solid phase diffusion resistance and smaller particle surface flux. The discharge at the C/1.3 rate shown in Fig. 9 reaches the end of discharge voltage before the phase transition occurs throughout the electrode. But at lower discharge rates, the electrode may experience all the phase transition stages shown in Fig. 7. Simulations show that the phase transition also ends first in the particles close to the separator (Fig. 7d). The simulated flux distribution indicates that the nonuniformity of the flux distribution reaches its maximum just before phase transition ends at the separator side. Then the flux distribution gradually levels off as the phase transition progressively ends in the electrode.

Figure 11 shows the simulated discharge profiles obtained with a normal porous electrode model which does not use a moving boundary model to account for the phase transition in the solid phase particles. The $LiCoO_2$ particles are assumed to be occupied by α phase only during the entire discharge process. The same parameters listed in Table I are used in the simulation. The normal porous electrode model could well predict the experimental discharge curves when the entire electrode is in single α phase stage (Fig. 7a). But it cannot predict the large potential drop after phase transition happens in the $LiCoO_2$ electrode at high current rates. In addition, the discharge capacities predicted by the normal porous electrode model are much higher than the experimental ones. The reason is that the normal model does not consider the formation of Li rich β

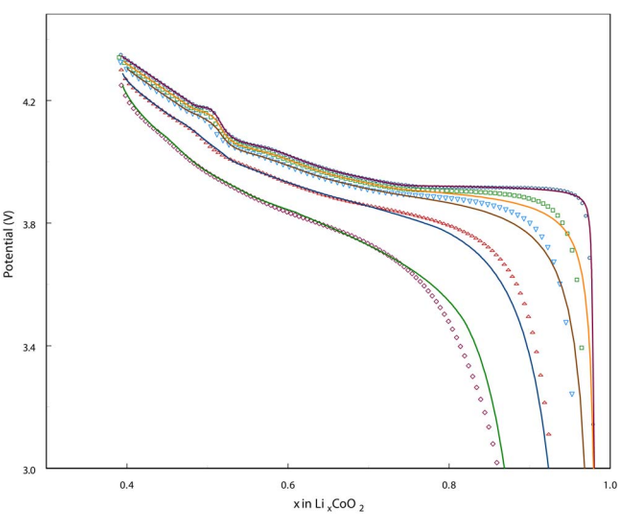

Figure 8. (Color online) Comparison of experimental (symbols) and simulated (lines) discharge profiles of the $LiCoO_2$ electrode. Moving boundary model coupled with porous electrode model is used in the simulation. The discharge rates from the top to the bottom are about C/66, C/13, C/7, C/2.7, and C/1.3 (C = 4 mA).

Table I. Summary of model equations.

	$x = 0$	$0 < x < \delta_p$	$x = \delta_p$	$\delta_p < x < \delta_p + \delta_s$	$x = \delta_p + \delta_s$
c_e	$-D_e^{\text{eff}}\frac{\partial c_e}{\partial x} = 0$	$\frac{\partial \varepsilon_e c_e}{\partial t} - \nabla \cdot (D_e^{\text{eff}} \nabla c_e) - \frac{1 - t_+^0}{F} a_s j_n = 0$	$-D_e^{\text{eff}}\frac{\partial c_e}{\partial x}\|_{x=\delta_p^-} = -D_e^{\text{eff}}\frac{\partial c_e}{\partial x}\|_{x=\delta_p^+}$	$\frac{\partial \varepsilon_e c_e}{\partial t} - \nabla \cdot (D_e^{\text{eff}} \nabla c_e) = 0$	$\frac{I}{S}\frac{1}{F}(1 - t_+^0) = -D_e^{\text{eff}}\frac{\partial c_e}{\partial x}$
ϕ_s	$-\sigma_s\frac{\partial \phi_s}{\partial x} = \frac{I}{S}$	$\nabla \cdot (\sigma_s \nabla \phi_s) - a_s j_n = 0$	$-\sigma_s^{\text{eff}}\frac{\partial \phi_s}{\partial x}\|_{x=\delta_p^-} = 0$		
ϕ_e	$-\kappa_e^{\text{eff}}\frac{\partial \phi_e}{\partial x} = 0$	$\nabla \cdot \left(\kappa_e^{\text{eff}} \nabla \phi_e - \frac{2RT\kappa_e^{\text{eff}}}{F}\upsilon \nabla \ln c_e\right) = -a_s j_n$ where $\upsilon = (1 - t_+^0)\left(1 + \frac{d \ln f_\pm}{d \ln c_e}\right)$	$-\kappa_e^{\text{eff}}\frac{\partial \phi_e}{\partial x}\|_{x=\delta_p^-} = -\kappa_e^{\text{eff}}\frac{\partial \phi_e}{\partial x}\|_{x=\delta_p^+}$	$\nabla \cdot \left(\kappa_e^{\text{eff}} \nabla \phi_e - \frac{2RT\kappa_e^{\text{eff}}}{F}\upsilon \nabla \ln c_e\right) = 0$ where $\upsilon = (1 - t_+^0)\left(1 + \frac{d \ln f_\pm}{d \ln c_e}\right)$	$\frac{I}{S} = -i_{0,\text{Li}}\left[\exp\left(\frac{0.5F}{RT}(-\phi_e)\right) - \exp\left(\frac{-0.5F}{RT}(-\phi_e)\right)\right]$
j_n	$j_n = i_0\left(\exp\left(\frac{\alpha_a F}{RT}(\phi_s - \phi_e - U_{\text{eq}})\right) - \exp\left(-\frac{\alpha_c F}{RT}(\phi_s - \phi_e - U_{\text{eq}})\right)\right)$, where $i_0 = k_i c_e^{\alpha_a}(c_{\max} - c\|_{r=R_s})^{\alpha_a} c\|_{r=R_s}^{\alpha_c}$				
	α only	$\frac{\partial c_\alpha}{\partial t} = \frac{1}{r^2}\left(D_\alpha r^2 \frac{\partial c_\alpha}{\partial r}\right)$, $-D_\alpha \frac{\partial c_\alpha}{\partial r}\|_{r=0} = 0$, $-D_\alpha \frac{\partial c_\alpha}{\partial r}\|_{r=R_s} = \frac{j_n}{F}$			
		α: $[ur(t)]^2\left(\frac{\partial c_\alpha}{\partial t} - \frac{u}{r(t)}\frac{dr(t)}{dt}\frac{\partial c_\alpha}{\partial u}\right) = \frac{\partial}{\partial u}\left(D_\alpha \frac{(ur(t))^2}{r(t)^2}\frac{\partial c_\alpha}{\partial u}\right)$, $-D_\alpha \frac{\partial c_\alpha}{\partial u}\|_{u=0} = 0$, $c_\alpha\|_{u=1} = c_{\text{eq},\alpha}$			
c	α + β	$r(t)$: $\frac{D_\alpha}{r(t)}\frac{\partial c_\alpha}{\partial u}\|_{u=1} - \frac{D_\beta}{R_s - r(t)}\frac{\partial c_\beta}{\partial v}\|_{v=0} = [c_{\text{eq},\beta} - c_{\text{eq},\alpha}]\frac{dr(t)}{dt}$			
		β: $[v(R_s - r(t)) + r(t)]^2\left(\frac{\partial c_\beta}{\partial t} - \frac{1 - v}{R_s - r(t)}\frac{dr(t)}{dt}\frac{\partial c_\beta}{\partial v}\right)$ $= \frac{\partial}{\partial v}\left(D_\beta \frac{[v(R_s - r(t)) + r(t)]^2}{[R_s - r(t)]^2}\frac{\partial c_\beta}{\partial v}\right)$, $c_\beta\|_{v=0} = c_{\text{eq},\beta}$, $-D_\beta \frac{\partial c_\beta}{\partial v}\|_{v=1} = \frac{j_n}{F}(R_s - r(t))$			
	β only	$\frac{\partial c_\beta}{\partial t} = \frac{1}{r^2}\left(D_\beta r^2 \frac{\partial c_\beta}{\partial r}\right)$, $-D_\beta \frac{\partial c_\beta}{\partial r}\|_{r=0} = 0$, $-D_\beta \frac{\partial c_\beta}{\partial r}\|_{r=R_s} = \frac{j_n}{F}$			

Table II. Model parameters used in the simulation.

Parameter	Value	Parameter	Value
	$LiCoO_2$ Electrode		
T (°C)	15[a]	σ_s (S/cm)	0.1[b]
W (g)	0.0245[a]	R_s (cm)	1×10^{-4}[b]
δ_p (cm)	64×10^{-4}[a]	α_a	0.5[b]
S (cm^2)	1.267[a]	α_c	0.5[b]
ε_e	0.30[a]	ε_s	0.60[c]
t_+^0	0.363[b]	Brug	3.65[c]
c_{max} (mol/cm^3)	5.1555×10^{-2}[b]	x_0	0.393[c]
	Phases		
	$i = \alpha$		$i = \beta$
D_i (cm^2/s)	1×10^{-9}[b]		2×10^{-11}[c]
k_i ($A/cm^2/(mol \cdot cm^3)^{1.5}$)	1×10^{-2}[c]		2.77×10^{-2}[c]
$c_{eq,i}$	$0.75 \times c_{max}$[a]		$0.975 \times c_{max}$[a]
	Separator		
$c_{e,0}$	1×10^{-3}[a]	S (cm^2)	1.267[a]
δ_s (cm)	25×10^{-4}	ε_e	0.46[a]
D_e	Eq. A-1[b]	κ_e	Eq. A-2[b]
$\upsilon = (1 - t_+^0)\left(1 + \frac{d \ln f_\pm}{d \ln c_e}\right)$	Eq. A-3[b]		

[a] Manufacturer data or experimental data.
[b] From Ref. 22-24 and 31.
[c] Values fit to experimental data.

phase in the particles which has much smaller diffusion coefficient than Li poor α phase. Our moving boundary model reveals that the discharge of the $LiCoO_2$ electrode is heavily impacted by the formation of β phase in the particles. That is, the discharge process becomes significantly limited by the solid phase diffusion after phase transition gradually occurs in the electrode. By comparing Fig. 11 with Fig. 8, one can see that the profiles predicted by the moving boundary model are significantly improved from those predicted by the normal porous electrode model. The flux distribution predicted by the normal porous electrode model is also compared with the one obtained with the moving boundary model at C/1.3 rate in Fig. 12. The two flux distributions show significant difference after phase transition occurs in the electrode. The flux distribution predicted by the normal model lacks the fine details revealed in the other one and is more severely perturbed. The comparison also reveals the importance of including the phase transition phenomenon in the model for a $LiCoO_2$ electrode.

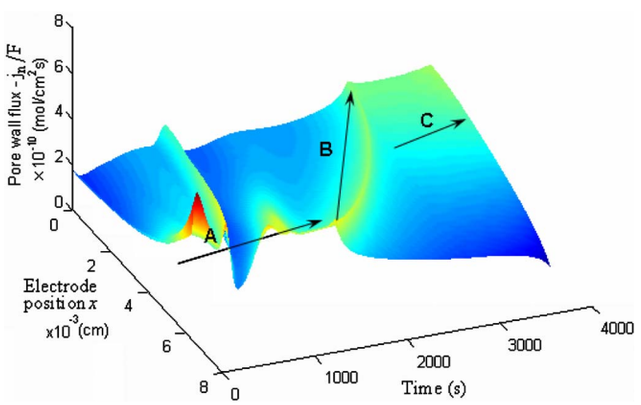

Figure 9. (Color online) The distribution of particle surface flux across the $LiCoO_2$ electrode at different times for the C/1.3 rate. The current collector is at $x = 0$. Refer to Fig. 7 for the phase transition sequence in the $LiCoO_2$ electrode during discharge. The ridge in stage B shows where the diffusion controlled phase transition occurs in a local particle along the electrode. The flux distribution is gradually shifted from being larger at the separator side to being larger at the current collector side because the phase transition changes the solid phase diffusion resistance across the electrode.

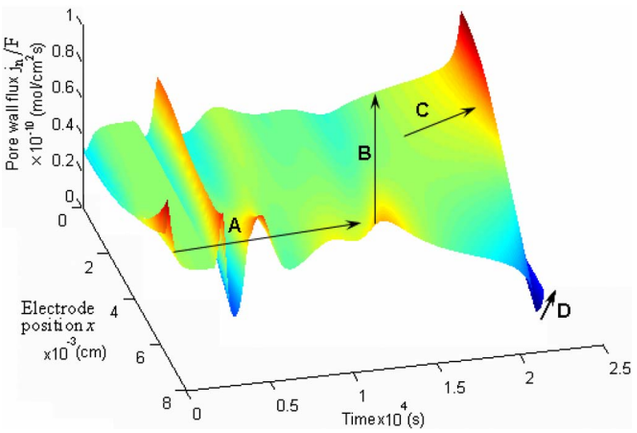

Figure 10. (Color online) The distribution of particle surface flux across the $LiCoO_2$ electrode at different times for C/7 rate. Phase transition ends in some part of the electrode (stage D) when reaching the end of discharge voltage at the C/7 rate.

Conclusion

A moving boundary model with two phases was presented and used to simulate experimental discharge curves for a $LiCoO_2$ electrode. The simulation results agree well with the experimental data. The phase transition phenomenon in the $LiCoO_2$ particles had a significant effect on the predicted flux distribution across the $LiCoO_2$ electrode because of the changing solid phase diffusion resistance along the electrode during phase transition. Model predictions from a normal porous electrode model which does not account for the phase transition in the solid phase particles were compared to those obtained with our moving boundary model. The comparison showed that it is important to incorporate phase transition with a moving boundary in the $LiCoO_2$ particles into the $LiCoO_2$ electrode model for high rates.

Acknowledgment

The authors are grateful for the financial support of the project by the National Reconnaissance Office (NRO) under contract no. NRO-000-03-C-0122.

The University of South Carolina assisted in meeting the publication costs of this article.

Appendix

This Appendix lists the electrolyte properties used in the simulation. The diffusion coefficient of the electrolyte was found to be[31]

$$\log(D_e) = -4.43 - 54/(T - 5 \times 10^3 c_e - 229) - 0.22 \times 10^3 c_e \quad [A\text{-}1]$$

The conductivity of the electrolyte was found to be[31]

$$\kappa_e = c_e\left(\begin{array}{l} -10.5 + 0.074T - 6.96 \times 10^{-5}T^2 + 668c_e \\ -17.8c_eT + 0.028c_eT^2 + 4.94 \times 10^5 c_e^2 - 886c_e^2T \end{array}\right)^2 \quad [A\text{-}2]$$

Bruggeman correlation was used to account for the effect of porosity and tortuosity on the transport properties of the electrolyte. The thermodynamic factor which accounts for the nonideality of the electrolyte was found to be[31]

$$\upsilon = (1 - t_+^0)\left(1 + \frac{d \ln f_\pm}{d \ln c_e}\right) = 0.601 - 7.59c_e^{0.5} + 3.1 \times 10^4(2.53 - 0.0052T)c_e^{1.5} \quad [A\text{-}3]$$

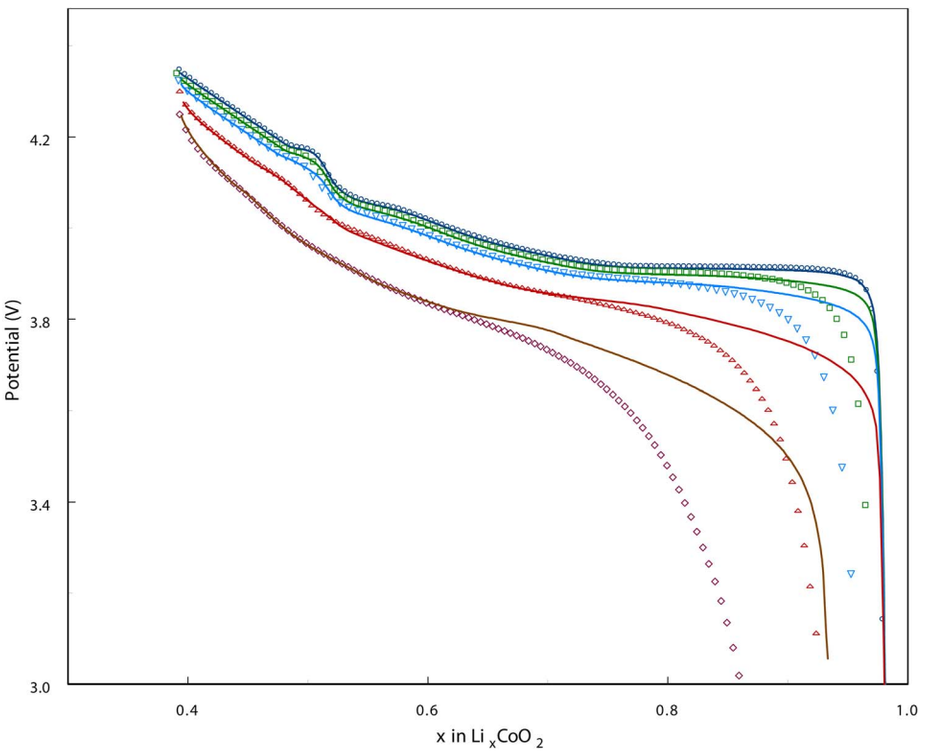

Figure 11. (Color online) Comparison of experimental (symbols) and simulated (lines) discharge profiles of the $LiCoO_2$ electrode. A normal porous electrode model (one without moving boundary model) is used in the simulation.

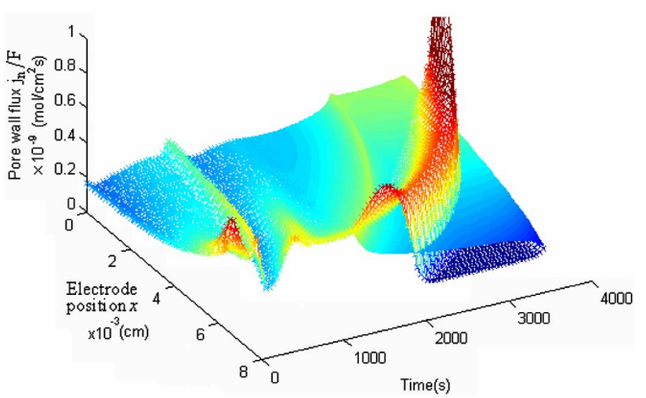

Figure 12. (Color online) Comparison of flux distributions in the $LiCoO_2$ electrode predicted by the moving boundary model (surface plot) and the normal porous electrode model (mesh plot with markers) at the C/1.3 rate.

List of Symbols

a_s	specific interfacial area of the electrode, cm^2/cm^3
Brug	Bruggeman coefficient
c	lithium concentration in $LiCoO_2$ particles, mol/cm^3
c_0	initial lithium concentration in $LiCoO_2$ particles, mol/cm^3
c_e	Li^+ concentration in the electrolyte, mol/cm^3
c_{eq}	equilibrium lithium concentration at the phase boundary, mol/cm^3
c_{max}	maximum lithium concentration in $LiCoO_2$ particles, mol/cm^3
C	current needed to completely discharge the electrode in an hour, C = 4 mA
D_i	diffusion coefficient of Li^+ in phase i, cm^2/s
D_e	diffusion coefficient of the electrolyte, cm^2/s
$f_\pm$	mean molar salt activity coefficient
F	Faraday's constant, 96487 C/mol
i_0	exchange current density, A/cm^2
I	discharge current, A
j_n	intercalation current density, A/cm^2
k	kinetic rate constant, (A/cm^2)/(mol/cm^3)$^{1.5}$
m	Number of discretization nodes in the r direction
n	number of discretization nodes in the x direction
Q	discharge capacity, Ah
$r(t)$	position of the phase boundary, cm
R	gas constant, 8.3145 J/mol · K
R_s	radius of $LiCoO_2$ particles, cm
S	geometric area of the electrode, cm^2
t	tme, s
t_+^0	transference number of the electrolyte
T	temperature, K
u	computational domain for α phase, $u = r/r(t)$, $0 \leqslant u \leqslant 1$
U_{eq}	equilibrium potential of the electrode, V
v	computational domain for β phase, $v = r - r(t)/R_s - r(t)$, $0 \leqslant v \leqslant 1$
W	active material loading in the electrode, g

Greek

α_a, α_c	Transfer coefficients
ϕ_e,ϕ_s	liquid or solid phase potential, V
δ_p,δ_s	electrode or separator thickness, cm
ε_e,ε_s	volume fraction of the electrolyte or active material in solid phase
κ_e	conductivity of the electrolyte, S/cm
σ_s	conductivity of the solid phase, S/cm
υ	thermodynamic factor of the electrolyte, Eq. A-3
Ω	physical domain of α or β phase in the particles

References

1. J. N. Reimers and J. R. Dahn, *J. Electrochem. Soc.*, **139**, 2091 (1992).
2. M. Yoshio, H. Tanaka, K. Tominaga, and H. Noguchi, *J. Power Sources*, **40**, 347 (1992).
3. T. Ohzuku and A. Ueda, *J. Electrochem. Soc.*, **141**, 2972 (1994).
4. M. Inaba, Y. Iriyama, Z. Ogumi, Y. Todzuka, and A. Tasaka, *J. Raman Spectrosc.*, **28**, 613 (1997).
5. Z. Chen, Z. Lu, and J. R. Dahn, *J. Electrochem. Soc.*, **149**, A1604 (2002).
6. W. Zhang, S. Srinivasan, and H. J. Ploehn, *J. Electrochem. Soc.*, **143**, 4039 (1996).
7. H. C. Shin and S. I. Pyun, *Electrochim. Acta*, **44**, 489 (1999).
8. H. C. Shin and S. I. Pyun, *Electrochim. Acta*, **44**, 2235 (1999).
9. V. R. Subramanian, H. J. Ploehn, and R. E. White, *J. Electrochem. Soc.*, **147**, 2868 (2000).
10. V. Srinivasan and J. Newman, *J. Electrochem. Soc.*, **151**, A1517 (2004).

11. D. M. Anderson, G. B. McFadden, and A. A. Wheeler, *Physica D*, **135**, 175 (2000).
12. B. C. Han, A. Van der Ven, D. Morgan, and G. Ceder, *Electrochim. Acta*, **49**, 4691 (2004).
13. J. S. Newman and K. E. Thomas-Alyea, *Electrochemical Systems*, 3rd ed., Prentice-Hall, Englewood Cliffs, NJ (2004).
14. M. Doyle, T. F. Fuller, and J. Newman, *J. Electrochem. Soc.*, **140**, 1526 (1993).
15. T. F. Fuller, M. Doyle, and J. Newman, *J. Electrochem. Soc.*, **141**, 1 (1994).
16. T. C. Illiingworth and I. O. Golosnoy, *J. Comput. Phys.*, **209**, 207 (2005).
17. H. G. Landau, *Q. J. Mech. Appl. Math.*, **8**, 81 (1950).
18. W. M. Murray and F. Landis, *Trans. ASME, Ser. B*, **81**, 106 (1959).
19. E. Javierre, C. Vuik, F. J. Vermolen, and S. van der Zwaag, *Comput. Appl. Math.*, **192**, 445 (2006).
20. K. E. Brenan, S. L. Campbell, and L. R. Petzold, *Numerical Solution of Initial Value Problems in Differential-Algebriac Equations*, Elsevier, New York (1989).
21. P. P. Prosini, *J. Electrochem. Soc.*, **152**, A1925 (2005).
22. M. Doyle and Y. Fuentes, *J. Electrochem. Soc.*, **150**, A706 (2003).
23. P. Ramadass, B. Haran, P. M. Gomadam, R. E. White, and B. N. Popov, *J. Electrochem. Soc.*, **151**, A196 (2004).
24. G. Ning, R. E. White, and B. N. Popov, *Electrochim. Acta*, **51**, 2012 (2006).
25. J. Barker, R. Pynenburg, R. Koksbang, and M. Y. Saidi, *Electrochim. Acta*, **41**, 2481 (1996).
26. J. M. McGraw, C. S. Bahn, P. A. Parilla, J. D. Perkins, D. W. Readey, and D. S. Ginley, *Electrochim. Acta*, **45**, 187 (1999).
27. H. D. Levi, G. Salitra, B. Markovsky, H. Teller, D. Aurback, U. Heider, and L. Heider, *J. Electrochem. Soc.*, **146**, 1279 (1999).
28. Y. I. Jang, B. J. Neudecker, and N. J. Dudney, *Electrochem. Solid-State Lett.*, **4**, A74 (2001).
29. A. Van der Ven, G. Ceder, M. Asta, and P. D. Tepesch, *Phys. Rev. B*, **64**, 184307 (2001).
30. N. J. Dudney and Y. I. Jang, *J. Power Sources*, **119–121**, 300 (2003).
31. L. O. Valoen and J. N. Reimers, *J. Electrochem. Soc.*, **152**, A882 (2005).